

# Volume and Shape Preservation via Moving Frame Manipulation

YARON LIPMAN, DANIEL COHEN-OR, GAL RAN, and DAVID LEVIN  
Tel Aviv University

---

This article introduces a method for mesh editing that is aimed at preserving shape and volume. We present two new developments: The first is a minimization of a functional expressing a geometric distance measure between two isometric surfaces. The second is a local volume analysis linking the volume of an object to its surface curvature. Our method is based upon the moving frames representation of meshes. Applying a rotation field to the moving frames defines an isometry. Given rotational constraints, the mesh is deformed by an optimal isometry defined by minimizing the distance measure between original and deformed meshes. The resulting isometry nicely preserves the surface details, but when large rotations are applied, the volumetric behavior of the model may be unsatisfactory. Using the local volume analysis, we define a scalar field by which we scale the moving frames. Scaled and rotated moving frames restore volumetric properties of the original mesh, while properly maintaining the surface details. Our results show that even extreme deformations can be applied to meshes, with only minimal distortion of surface details and object volume.

Categories and Subject Descriptors: I.3.5 [Computer Graphics]: Computational Geometry and Modeling

General Terms: Algorithms

Additional Key Words and Phrases: Mesh editing, moving frames, discrete differential geometry

## ACM Reference Format:

Lipman, Y., Cohen-Or, D., Ran, G., and Levin, D. 2007. Volume and shape preservation via moving frame manipulation. *ACM Trans. Graph.* 26, 1, Article 5 (January 2007), 14 pages. DOI = 10.1145/1186644.1186649 <http://doi.acm.org/10.1145/1186644.1186649>

---

## 1. INTRODUCTION

Triangular meshes are the *de facto* common representation of 3D objects in computer graphics. Recently, several researchers have studied the manipulation of meshes while preserving their surface details [Kobbelt et al. 1998; Yu et al. 2004; Lipman et al. 2004, 2005; Sorkine et al. 2004; Zhou et al. 2005]. The common idea in these works is to represent the surface with *differential coordinates*, and to minimize the changes in these coordinates under some constraints defining the editing objectives. One of the main issues is to find the quantities which should be preserved during the deformation. In previous works, the assumption was that preserving the differential coordinates which represent the local shape of the surface would lead to a detail-preserving operation. However, it has been noted that differential coordinates defined in a global coordinate system are not rotation-invariant, and as a result, the details in the deformed mesh are distorted. In Lipman et al. [2004], Yu et al. [2004], and Sorkine et al. [2004], it is shown that transforming the differential coordinates with respect to the given constraints alleviates the problem, provided that the deformations are not too large and the shapes not too complex.

Representing the surface by rotation-invariant differential coordinates [Lipman et al. 2005] decomposes the problem into finding the rotational transformation and residual general deformation. Solving first for the rotations and then for the positional constraints preserves the rigidity of the local details. The representation, introduced by Lipman et al. [2005], is based on moving frames encoded by differential values. Their technique is particularly attractive since it only requires solving two sequential linear least-squares systems. However, the geometric relevance of the quantity minimized in this process remains unclear. Moreover, the linear least-squares solution is not optimal, and under large deformations the shape of the model and its volume may be quite distorted. Furthermore, the deformation operators for over  $\pi$  radians are undefined, and can only be realized by a series of operators of smaller angles.

Drawing upon the moving frames representation, we introduce in the article a new mathematical framework which leads to a new method for mesh editing, aiming at the preservation of shape and volume. We developed two transformation fields that are applied to the moving frames, which in turn are used for the reconstruction of the deformed surface. The first is an optimal *rotation* field that preserves the surface local shape, and the second is a *scaling* field

---

Authors' addresses: Y. Lipman, School of Mathematical Sciences, Tel Aviv University, P.O. Box 39040, Tel Aviv 69978, Israel; email: lipmany@post.tau.ac.il; D. Cohen-Or, School of Computer Science, Tel Aviv University, P.O. Box 39040, Tel Aviv 69978, Israel; email: dcor@tau.ac.il; G. Ran, School of Computer Science, Tel Aviv University, P.O. Box 39040, Tel Aviv 69978, Israel; email: galran@post.tau.ac.il; D. Levin, School of Mathematical Science, Tel Aviv University, P.O. Box 39040, Tel Aviv 69978, Israel; email: levin@tau.ac.il.

Permission to make digital or hard copies of part or all of this work for personal or classroom use is granted without fee provided that copies are not made or distributed for profit or direct commercial advantage and that copies show this notice on the first page or initial screen of a display along with the full citation. Copyrights for components of this work owned by others than ACM must be honored. Abstracting with credit is permitted. To copy otherwise, to republish, to post on servers, to redistribute to lists, or to use any component of this work in other works requires prior specific permission and/or a fee. Permissions may be requested from Publications Dept., ACM, Inc., 2 Penn Plaza, Suite 701, New York, NY 10121-0701 USA, fax +1 (212) 869-0481, or [permissions@acm.org](mailto:permissions@acm.org).  
© 2007 ACM 0730-0301/2007/01-ART5 \$5.00 DOI 10.1145/1186644.1186649 <http://doi.acm.org/10.1145/1186644.1186649>



Fig. 1. The elephant model is deformed in one step with a  $2\pi$  rotation applied to the tip of his trunk.

that preserves the local volume. The new technique allows applying large deformations in a single step, while preserving both the shape and volume of the subject. Figure 1 shows an example of a large rotation ( $2\pi$  radians) applied to the trunk of an elephant. Another, more general deformation is shown in Figure 4.

### 1.1 Our Approach and Contributions

A shape is a geometric property that is invariant to rigid transformations. As such, a shape can be characterized by differential invariants of rigid transformations. In surface differential geometry, the first and second fundamental forms are used as such invariants, which form a complete local representation. Our approach to preservation of shape under a deformation that is subject to geometrical constraints is to look for a deformation which maintains the first fundamental form intact (an isometry), and minimizes changes in the second fundamental form. This leads to defining a distance measure  $Dist(M, \tilde{M})$  between two isometric surfaces  $M$  and  $\tilde{M}$  based on differences of the corresponding second fundamental forms. Thus, we are looking for *shape-preserving isometries*, which are isometric deformations that minimize the distance measure (see Figure 2).

Given a surface  $M$  and set of rotational constraints, we look for a deformation  $\tilde{M} = f(M)$  minimizing  $Dist(M, f(M))$ , where  $f$  is an isometric map that satisfies the prescribed constraints. Inspired by Cartan's moving frames theory [do Carmo 1994; Ivey and Landsberg 2003], we show a reduction of this problem to minimizing a Dirichlet-type integral, for which we devise an efficient solution.

Shape-preserving deformations tend to preserve volume better than other mesh deformation techniques. However, large deformations may still lead to undesirable volume changes. We introduce a method that scales the local frames to compensate for volume changes. Our approach is based on the general Stokes' theorem, using a carefully designed differential form which establishes a connection between *local volume* and surface properties. Our approach avoids the explicit construction of any volumetric representation

and its inevitable cubic complexity. It enables volume correction by merely scaling the moving frames on the surface.

## 2. BACKGROUND

Deforming shapes has been intensively investigated in the context of interactive editing (e.g., Kobbelt et al. [1998], Botsch and Kobbelt [2004]) and shape blending (e.g., Igarashi et al. [2005], Xu et al. [2005]). The main challenge is to handle nontrivial transformations, that is, transformations which include rotations (especially large rotations) while preserving as much as possible the visual characteristic of the shape at interactive rates.

In shape blending, it has been accepted that deforming shapes *as rigid as possible* provides plausible results. The key idea is to factor out the rotation from the deformation. Since rotations are rigid transformations, such factorization enables treating the deformation as pure rotation plus a residual elastic deformation. Cohen-Or et al. [1998] have applied this concept to minimize the global deformation during shape interpolation.

Alexa et al. [2000] show how this can be applied locally as a means of treating the volume (area) of a shape as rigid as possible. Xu et al. [2005] have recently extended these principles to the surface of a shape. They factor out rotations of the transformed triangles and have shown that the volume of the interpolated mesh is well behaved.

In the context of shape editing, the problem of factoring out the rotation turns out to be significantly harder. Since the target shape is not explicitly given (as in a shape interpolation setting) the factorization and shape definition have to be solved simultaneously [Sorkine et al. 2004]. Recently, Huang et al. [2006] and Botsch et al. [2006] have successfully introduced algorithms based on nonlinear formulations. Huang et al. [2006] used a subspace domain to reduce the problem dimensionality via mean value coordinates [Floater 2003; Ju et al. 2005]. Botsch et al. [2006] introduced a local shape representation based on prisms and used a hierarchical multigrid solver to reduce the problem complexity.

Instead of factoring out the rotation, a better solution is to represent the shape with intrinsic [Sederberg et al. 1993] or rotation-invariant coordinates [Lipman et al. 2005]. With purely rotation-invariant coordinates, the factorization of the rotation is given for free. Lipman et al. [2005] proved that by representing the mesh vertices within their own local frames, it is possible to uniquely represent a mesh, and that its reconstruction merely requires solving a sequence of two linear systems. However, the least-squares solution for rotations is not optimal. For large deformations, it may cause counterintuitive distortions to the surface, and consequently, implausible deformations (see Figure 8). Zayer et al. [2005] used a harmonic scalar field to better propagate deformations to the entire mesh from the constraints. They use a scalar harmonic field that ranges from one at the handles to zero on the fixed vertices constraints to interpolate the quaternions representing global rotations.

A different research direction aims at preservation of the volume of a shape. The prominent approach directly enforces volume preservation through an explicit construction of a representation that models the interior of the shape (e.g., Rappaport et al. [1995], Aubert and Bechmann [1997], Hirota et al. [1999], Botsch and Kobbelt [2003], and Zhou et al. [2005]). A common approach to solving a physically-based model is the finite element method (FEM) [Bathe 1982]. With these methods, the shape can be accurately preserved by simulating the behavior of the deformed volume. These techniques model the entire volume of objects and solve the deformation in small time steps. Given a detailed surface, the construction of the elements is quite involved. Furthermore, to allow interactive times, typically only a relatively small number of elements are modeled.

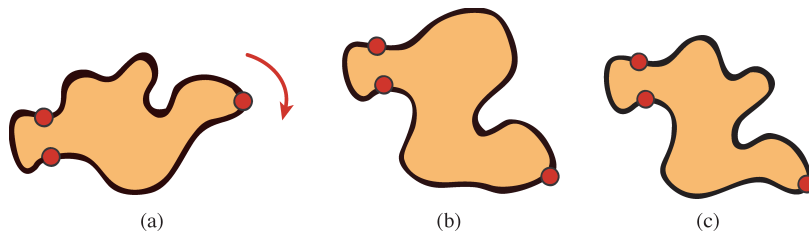


Fig. 2. Illustration of two isometric deformations (b) and (c) of the shape in (a). The two deformations are isometric, as they both preserve the length of the perimeter. However, the shape in (c) better preserves the shape of (a) in the sense that the curvature of corresponding points (along the arc length) are better preserved than in (b).

Another problem is the nonlinearity of the strain function. To alleviate the problem, some approximations can be used; for example, Muller et al. [2002] approximate the stiffness matrix of the strain function at each time step using a warping of the original stiffness matrix by a rotation field.

Recently, Zhou et al. [2005] developed a mesh deformation that strives to preserve the local volume. They build an internal structure of points with neighboring relations. While their construction is simpler than a tetrahedral structure, its complexity is still cubic in the general case. To propagate the transformation of the handle, they use a geodesic distance field, which may lead to counterintuitive results for large-scale details [Zayer et al. 2005; Lipman et al. 2005].

The aforementioned methods require explicit representation of the solid/volume of the manipulated object. The approach that we introduce in this article is different, since the volume is merely represented implicitly, and therefore, runtime computation uses surface information only, hence, remains proportional to the size of the surface representation, rather than its volume.

Botsch and Kobbelt [2003] introduce a method for volumetric detail-preservation based on the multiresolution paradigm by using volume elements (prisms) between the surface and its smooth version. They employ hierarchical relaxation to solve a nonlinear system, which corrects the position of surface vertices to optimize the local volume.

Angelidis et al. [2004] introduce a unique editing tool that preserves volume. It is based on an operator, called swirling-sweepers, which is applied along a path where in each incremental step, the swirl locally twists the space around while preserving the volume. This tool gives the artist the illusion that he is interacting with real material, like, for example, clay. Recently, von Funck et al. [2006] used a divergence-free vector field to define a shape-preserving editing operator.

### 3. ISOMETRIC SHAPE-PRESERVING DEFORMATIONS

In this section we formulate the theoretical background to the construction of a surface deformation technique (which best preserves geometric properties) aiming at minimizing distortion of the shape. We define a rigid motion-invariant geometric distance between two isometric surfaces. Then, given a surface and a set of rotational constraints, we look for an isometric deformation minimizing the geometric distance to the original surface under the constraints. We show that this minimization problem can be reduced, using notions from Cartan's moving frames theory, to a Dirichlet energy functional in  $SO(3)$  (the rotation group in  $\mathbb{R}^3$ ). The application of this theory to meshes employs the finite element approach to minimizing the energy functional.

A well-known result in differential geometry is that the first and second fundamental forms uniquely define a surface up to rigid transformation. We can thus regard the first and second fundamental forms as complete local descriptors of a surface. Since we deal with isometries, and the first fundamental form (which defines the metric on the surface) is invariant under isometric deformations, we consider only the second fundamental form. The second fundamental form, defined from the normal map differential, describes the local sectional curvature of the surface (curvature tensor). In other words, it describes the local change of the normal, or in formal terms, it is the quadratic form defined by the normal differential, namely, the *shape operator*. Thus, minimizing the *change* in the second fundamental form yields an overall minimal shape distortion of an isometry. As we shall see, the change in the normal differential can be measured by the differential of rotations applied to moving frames. Hence, minimizing the integral norm of the differential of the rotations field over the surface yields a least-distorting isometry.

#### 3.1 Least-Distorting Isometric Deformations—The Smooth Case

Let  $M$  and  $\tilde{M}$  be two differentiable isometric surfaces embedded in  $\mathbb{R}^3$  with the induced metric from the Euclidian ambient space  $\mathbb{R}^3$ , which we denote by  $\langle \cdot, \cdot \rangle_p$ ,  $p \in M$ . Let  $T_p M$  denote the tangent plane to  $M$  at point  $p$ . Denote by  $f : M \rightarrow \tilde{M}$  the isometry map between the surfaces. Let  $(e_1, e_2, e_3) : V \subset M \rightarrow \mathbb{R}^3$  be a *moving frame* on a patch of the surface  $V \subset M$ . In other words,  $(e_1(p), e_2(p), e_3(p))$  is a smooth orthonormal frame such that  $e_1(p), e_2(p)$  spans the tangent plane  $T_p M$  at each point  $p \in V \subset M$ , and  $e_3(p)$  is normal to the surface.

The isometry  $f$  induces a moving frames field on  $\tilde{M}$ :  $\tilde{e}_1 = df_p(e_1)$  and  $\tilde{e}_2 = df_p(e_2)$ , where  $df$  is the differential of  $f$ , that is,  $df_p(\xi)$  stands for the derivative of  $f$ , at the point  $p \in M$ , in the direction of  $\xi \in T_p M$ . The vector  $\tilde{e}_3$  is defined uniquely so that  $(\tilde{e}_1, \tilde{e}_2, \tilde{e}_3)$  has a positive orientation (see Figure 3).

At each point  $p \in V \subset M$ , we denote by  $H = H_p = (h_{i,j})_{i,j=1,2}$  the matrix representation of the differential of  $e_3$  at  $p$ . Phrased differently,  $(de_3)_p$  in the basis  $e_1(p), e_2(p)$  of  $T_p M$ . The normal map  $e_3(p)$ ,  $p \in V$  is also known as the *Gauss map* and the differential of this map is known as the *shape operator*.  $\tilde{H}$  is similarly defined in the basis  $\tilde{e}_1(f(p)), \tilde{e}_2(f(p))$  of  $T_{f(p)} \tilde{M}$ . Since  $e_1(p), e_2(p)$  is an orthonormal basis of  $T_p M$ , the matrix  $H$  is also the matrix of the second fundamental form in this basis, where the second fundamental form is defined as  $\langle H\xi, \xi \rangle_p$ , where  $\xi \in T_p M$  is represented in the basis  $(e_1, e_2)$ .

The local geometric distance between isometric surfaces is defined by the distance between the corresponding normal maps' differential matrices  $H$  and  $\tilde{H}$ . Let us use the Frobenius norm

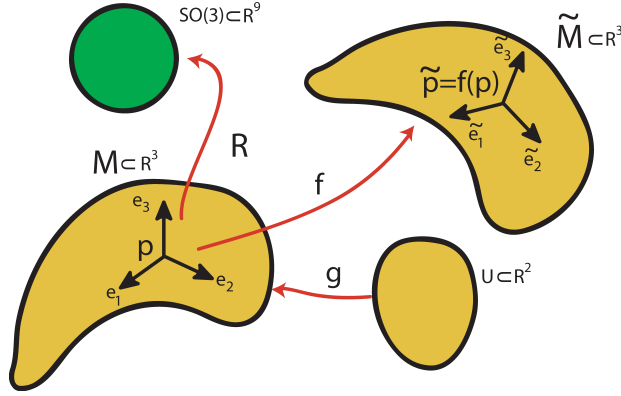


Fig. 3. The setup for shape-preserving isometric deformation of surfaces.

$\|A\|^2 = \sqrt{\sum_{i,j} |a_{i,j}|^2} = \text{trace}(A \cdot A^T)$  to define a *local geometric distance* as

$$\text{dist}_{M,f}^E(p) = \|H - \tilde{H}\|_F^2, \quad (1)$$

where  $E = (e_1, e_2, e_3)$  denotes the moving frame  $E$  used. As proved in Lemma C.1 (in Appendix C), the function  $\text{dist}_{M,f}^E$  is invariant to the choice of the moving frame, that is, depends only on  $M$  and the isometry  $f$ . Hence, this function is well-defined, and hereafter we denote this function by  $\text{dist}_{M,f}$ .

Integrating  $\text{dist}_{M,f}$  over the surface  $M$  yields a rotation-invariant *geometric distance*,

$$\text{Dist}(M, f(M)) = \text{Dist}_{M,f} = \int_M \text{dist}_{M,f} d\sigma, \quad (2)$$

where  $d\sigma$  is the area element. Since a surface is determined up to rigid motion by its fundamental forms,  $\text{Dist}_{M,f} = 0$  if and only if  $M$  and  $f(M) = \tilde{M}$  are rigid motion of each other. Therefore, we claim that this distance measures to what extent the surface  $M$  and deformed surface  $\tilde{M}$  are rigid motion of each other. It is important to note that this latter property of geometric measure cannot be achieved by using only the Gauss and mean curvatures. As a simple example, the well-known Catenoid and Helicoid shapes have an isometric correspondence between them such that at corresponding points, the Gauss and mean curvatures are the same, but the surfaces are clearly not a rigid motion of each other [Ivey and Landsberg 2003]. It turns out that  $(\text{Dist}_{M,f})^{1/2}$  can be used to define a metric between isometric surfaces. However, in this work we are simply using  $\text{Dist}_{M,f}$  as a distance measure.

Now we are ready to define our *geometric deformation problem*: Given a surface  $M$ , the goal is to deform it into a surface  $\tilde{M}$ , subject to some prescribed constraints such that the geometric distance between  $M$  and  $\tilde{M}$  is minimal.

Usually, minimizing the geometric distance integral may be extremely difficult. Fortunately, the problem can be reduced to a known problem of minimizing a Dirichlet-type integral. Consider a rotation field  $R : M \rightarrow SO(3)$ , where  $SO(3)$  is the rotation matrix group on  $\mathbb{R}^3$  embedded in  $\mathbb{R}^9$  with the induced metric from ambient Euclidean space  $\mathbb{R}^9$  (see Figure 3). Here,  $R \in SO(3)$  is defined at any point  $p \in M$  such that  $Re_i = \tilde{e}_i$ ,  $i = 1, 2, 3$ . In Appendix A, we show that  $\|H - \tilde{H}\|_F^2 = 1/2 \|\nabla R\|_F^2$ , hence we obtain the following representation for the geometric distance:

$$\text{Dist}_{M,f} = \frac{1}{2} \int_M \|\nabla R\|_F^2 d\sigma. \quad (3)$$

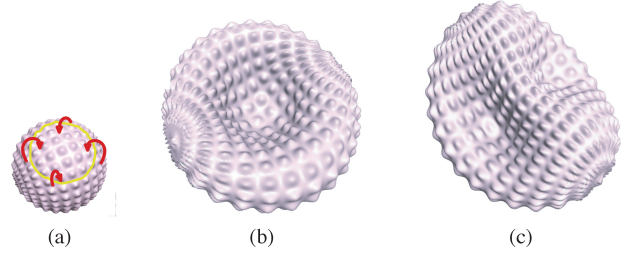


Fig. 4. A general deformation is applied to a bumpy sphere. In (a), the handle set is drawn (yellow) over the original model; (b) is the result of applying the deformation, and (c) is the result of applying two such deformations.

Therefore, the distance function is reduced to an energy functional on the rotation's field  $R$ . In other words, the amount of shape distortion by the isometry  $f$  is low iff the energy of the rotation field is low. The minimizer of the integral on the right-hand side, subject to constraints, is a generalization of the classical harmonic map functions to maps into Lie groups ( $SO(3)$  in our case). The type of constraints we consider are rotational constraints, that is, the rotations are prescribed on a subset  $C \subset M$ .

Based on the preceding, the geometric deformation problem is realized by the following two steps:

- Compute a rotation field  $R : M \rightarrow SO(3)$  such that  $\int_M \|\nabla R\|_F^2 d\sigma$  is minimized subject to constraints  $R|_C = R_0$ .
- Apply rotations over the moving frames, and reconstruct the isometry  $f$ .

### 3.2 Parametrization of $SO(3)$

Since the images of  $R$  are rotations, we need to use a parametrization of  $SO(3)$ . There is no canonical parametrization of this group, hence we suggest two parametrizations, each of which is advantageous in different cases.

In the case where rotational constraints in the geometric deformation problem share the same axes of rotation, the solution to our variational problem can be further reduced. Using an orthogonal parametrization of  $SO(3)$  (as described in Appendix D) with coordinates  $(\theta^1, \theta^2, \theta^3)$ , where  $\theta^1$  describes the angle of rotation around the axis of rotation, the integral in Eq. (3) takes the form:

$$2 \int_M \|\nabla \theta^1\|^2 + 4 \sin^2\left(\frac{\theta^1}{2}\right) (\|\nabla \theta^2\|^2 + \sin^2(\theta^2) \|\nabla \theta^3\|^2) d\sigma. \quad (4)$$

When all the constrained rotations  $R_0(p)$ ,  $p \in C$  have the same rotation axis, they can be represented by  $\theta^2 = 0 = \theta^3$ . Hence, an immediate consequence of this representation is that there is a minimizer such that  $\theta^2 \equiv 0$  and  $\theta^3 \equiv 0$ . Therefore, we are left with the problem of minimizing  $\int_M \|\nabla \theta^1\|^2 d\sigma$ , which leads to the linear (sparse) Laplace-Beltrami operator. For example, bending deformations such as those shown in Figures 1, 5, 6, and 15 are of this type. Thus, we note that in such deformations, the minimizer is obtained when the rotation angle  $\theta^1$  is harmonic. Specifically, it enables applying a rotation of more than  $2\pi$  in a single step. At this point, we note that in the case of a single rotation axis, applying the technique of Zayer et al. [2005], that is, using harmonic scalar field to interpolate the quaternions, results in the same rotation field as in our method.

In the general setting, where the rotational constraints consist of different rotation axes, the minimization leads to nonlinear Euler-Lagrange equations. However, with conformal parametrizations of

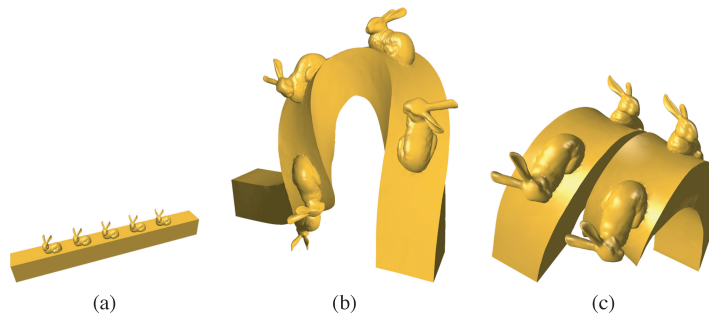


Fig. 5. A bar with bunnies (a) (110K polygons) is deformed in (b) by two rotations of  $3\pi/2$  each. In (c), a single large rotation of  $3\pi$  is applied.

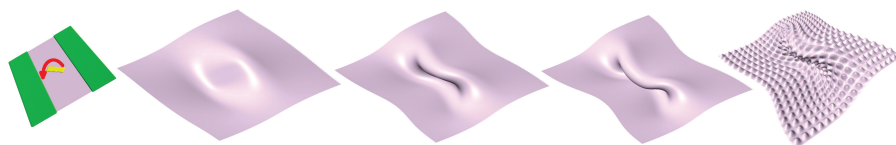


Fig. 6. A plane is deformed into a wavy shape using the (yellow) handle set in the middle, and identity boundary conditions are set at the (green) boundary of the plane.

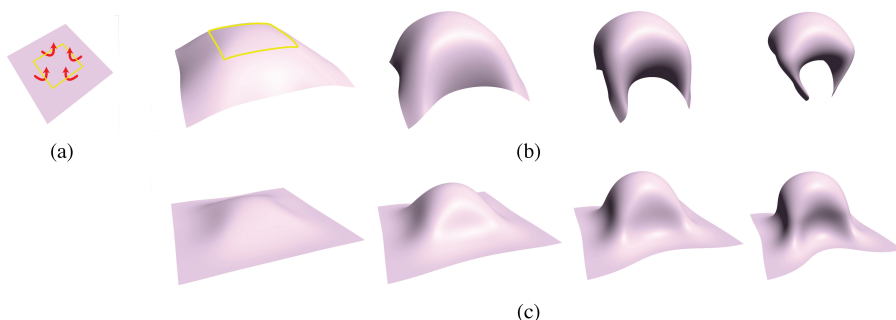


Fig. 7. A demonstration of the effect of different boundary conditions; (a) the initial plane with the square handle (in yellow) placed around its center. The axis of rotations around the handle are tangents to the handle curve; (b) a series of rotations of  $0, \pi/6, \pi/3, \pi/2, 2\pi/3$  radians around the axis of rotation, where the (identity) boundary conditions are weakened by a factor of 0.01; (c) a series of the same rotations, but with (identity) boundary rotations now factored by 1.0, and hence, keeping the boundary of the planar shape with the original orientation.

$SO(3)$  (Appendix D), the integral in Eq. (3) takes the form:

$$64 \int_M \frac{1}{(4 + \|\bar{\eta}\|^2)^2} \|\nabla \bar{\eta}\|^2 d\sigma, \quad (5)$$

where  $\bar{\eta} = (\eta^1, \eta^2, \eta^3)$  are the conformal coordinates. As shown next, this representation is advantageous in applications, that is, we derive an iterative scheme where the first (linear) solution is already a good approximation of the minimizing rotation field. Note that in this case, it is impossible to represent rotations with rotation angle of over  $2\pi$ , without introducing ambiguity, therefore in this case, the deformation should consist of angles smaller than  $2\pi$ .

To find the deformed surface  $\tilde{M}$ , we need to integrate the computed rotation field  $R$  using the relation  $df = R$ . However, such an integration is well-defined only if  $R$  satisfies certain compatibility conditions. Rotation fields which minimize the energy functional (3), under some constraints, do not necessarily satisfy the compatibility conditions. Therefore, we adopt the approach used in Lipman et al. [2005] to find the transformation  $f$  such that  $\|df - R\|$  is min-

imized. The actual application of this step to meshes is described in Section 5.

### 3.3 Piecewise-Linear Case

In practice, we want to apply geometric deformation to piecewise-linear surfaces. Given a two-manifold *mesh*, denoted by  $M$ , we would like to deform it into a mesh  $\tilde{M}$  subject to constraints  $R(p) = R_0(p)$ ,  $p \in C \subset M$ . We shall minimize the geometric distance given by Eq. (3), ( $R : M \rightarrow SO(3)$ ) subject to the given constraints. We adopt the piecewise-linear finite element approach and approximate  $R$  by a linear function on every triangle  $T_i \in T$ , where  $T$  are the triangles of the mesh  $M$ , and minimize this with respect to values at the vertices. In particular, we minimize the geometric distance (Eq. (3)) with the approach used to minimize the Dirichlet energy functional in Euclidian spaces [Polthier 2005; Pinkall and Polthier 1993]. Here, it is extended to minimize the Dirichlet energy functional in the more general setting of maps into  $SO(3)$ .

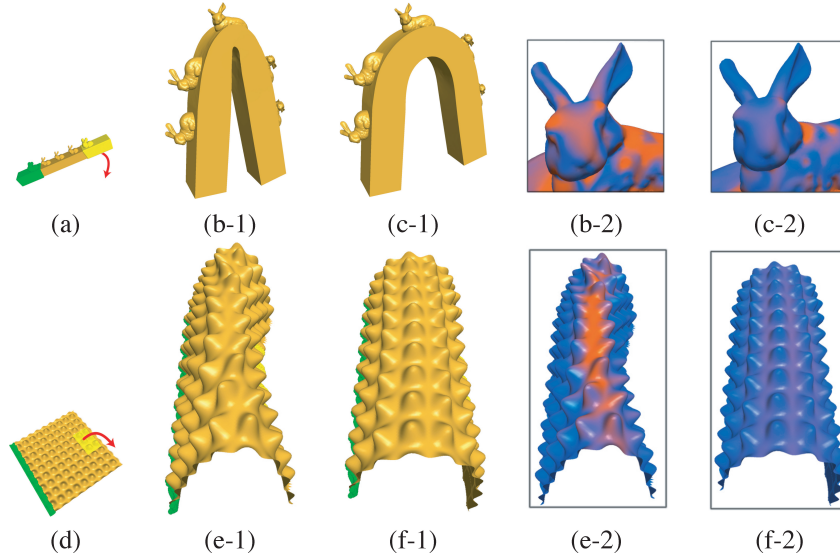


Fig. 8. A comparison with the method of Lipman et al. [2005]. The bar model is rotated by just less than  $\pi$  radians (a). On (b-1), a bar with bunnies is deformed by the technique of Lipman et al. [2005] and by our technique (c-1). Note how the error is evenly distributed by our technique. The colored close-up views (b-2),(c-2) of the bunny head show the differences in mean curvature with respect to the original shape. Another example is shown in (d),(e),(f) with a bumpy plane model.

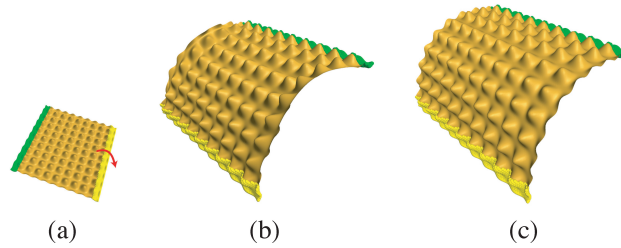


Fig. 9. A comparison with the method of Sorkine et al. [2004]. The bumpy plane is rotated by  $\pi/2$  radians (a). In (b), the method of Sorkine is applied, and in (c) our method is applied.

In the case of constraints sharing one rotation axis, the problem is reduced to minimizing  $\int_M \|\nabla\theta^1\|^2 d\sigma$ . Hence, the minimizing solution satisfies  $\Delta_M\theta^1 = 0$  on  $M$ , where  $\Delta_M$  is the Laplace-Beltrami operator. Following Polthier [2005] and Pinkall and Polthier [1993], the piecewise-linear approximation to  $\int_M \|\nabla\theta^1\|^2 d\sigma$  is given by  $Q = \sum_{T_i \in \mathcal{T}} Q_{T_i}$ , where  $Q_{T_i} = \sum_{j=1}^3 \cot \gamma_{i_j} |\theta_{i_{j+1}}^1 - \theta_{i_{j-1}}^1|^2$ , where  $i_1, i_2$ , and  $i_3$  are indices of the vertices of triangle  $T_i$ , and  $\gamma_{i_k}$  are the respective angles. We minimize  $Q$ , subject to the given constraints, by solving the corresponding sparse linear system:

$$\sum_{r \in N_j} (\cot(\alpha_j^r) + \cot(\beta_j^r)) (\theta_j^1 - \theta_r^1) = 0, \quad j \in V, \quad (6)$$

where  $N_j$  are the neighbors of vertex  $j$ , and  $\alpha_j^r, \beta_j^r$  are the angles opposite the edge  $(j, r)$ .

After solving for the rotations, we apply them to the moving frames and follow the paradigm in Lipman et al. [2005] to construct the deformed mesh  $\tilde{M}$  defined by these frames in the least-squares sense. The implementation details and results are described in Section 5.

In the general case of general rotational constraints, we use the conformal parametrization of  $SO(3)$  and the form (5) of  $Dist_{M,f}$ .

Integrating over the mesh, following Polthier [2005] and Pinkall and Polthier [1993] again, we get:

$$\int_M \frac{1}{(4 + \|\bar{\eta}\|^2)^2} \|\nabla\bar{\eta}\|^2 d\sigma = \frac{1}{6} \sum_{T_i \in \mathcal{T}} W_{(i_1, i_2, i_3)} Q_{T_i}, \quad (7)$$

where  $W_{(i_1, i_2, i_3)} = (w(\bar{\eta}_{i_1}) + w(\bar{\eta}_{i_2}) + w(\bar{\eta}_{i_3}))$  and  $w(\bar{\eta}) = 1/(4 + \|\bar{\eta}\|^2)^2$ . Differentiating with respect to each unknown  $\eta_j^l$  of vertex  $j$ , and equating zero, yields the following system:

$$\sum_{r \in N_j} \frac{2\eta_j^l}{(4 + \|\bar{\eta}_j\|^2)^3} (\cot(\alpha_j^r) W_{(j,r,r+1)} + \cot(\beta_j^r) W_{(j,r,r-1)}) (\eta_j^l - \eta_r^l) = \sum_{T_i \in NT_j} Q_{T_i}, \quad (8)$$

where  $NT_j$  are neighboring triangles to vertex  $j$ , respectively.

The system is solved by an iterative scheme where the nonlinear part is calculated using the previous iteration. The initial guess is chosen to be identically zero. In practice, the convergence of the system is fast (few iterations are enough), where typically a single iteration already yields close enough results, as shown in Figure 10. Note that a single iteration is equivalent to solving Eq. (6) for each of the conformal coordinates  $(\eta^1, \eta^2, \eta^3)$ .

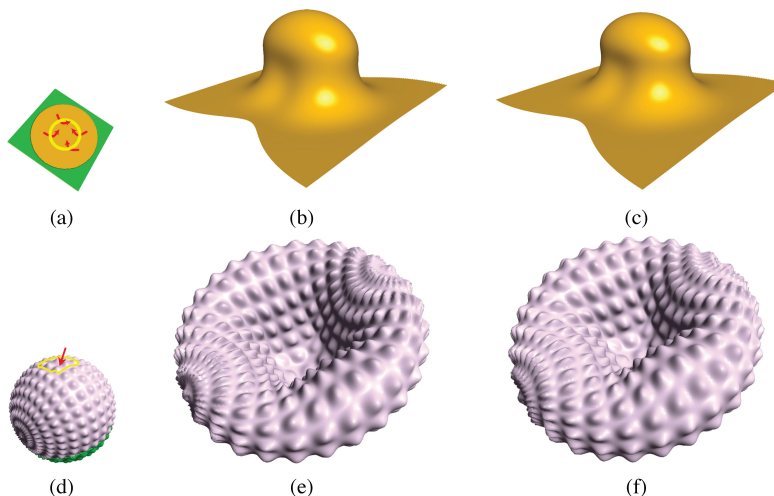


Fig. 10. A demonstration of the difference between the convergent solution of the iterative process and the first (linear) approximation of the general geometric deformation problem; (a) the initial plane with the circle handle drawn around its center (in yellow) and the static set colored in green. The axis of rotations around the handle are tangents to the handle curve and the angle of rotation is approximately  $2\pi/3$ ; (b) the result after the first (linear) iteration; and (c) the convergent result achieved after ten iterations. Note how well the linear solution approximates the convergent solution. In (d)–(f), another example where (e) is the linear first solution and (f) is the convergent solution.

## 4. VOLUME PRESERVATION

It is well known that isometric deformation of closed surfaces may cause undesired volume distortions. In this section we deal with volume correction and focus on local volume preservation, which is visually more important than global volume preservation. The local volume is defined as an estimate of the volume below a surface element, in the direction of the inward normal. Preserving the local volume yields plausible shapes at the expense of a rather small distortion of the local surface area. Furthermore, our local volume preservation yields a good approximation to a global volume preservation, as we demonstrate in Section 5.

The isometries defined in the previous section dictate the desired rotations of the local frames. Here we introduce a means to control the local volume by scaling the moving frames, while retaining the local rotations intact.

The main idea is to derive an expression for the local volume in terms of surface curvature and local thickness, and to use this expression to modify the surface  $M$  accordingly. The emphasis is on achieving volume preservation by surface operations alone.

### 4.1 The General Idea

Stokes' theorem states that given a two-form  $\mu$  in a domain  $D \subset \mathbb{R}^3$  with smooth boundary  $\partial D$ ,

$$\int_D d\mu = \int_{\partial D} \mu,$$

where  $d$  denotes the exterior derivative [Stoker 1989; do Carmo 1994; Ivey and Landsberg 2003] of  $\mu$ .

Stokes' theorem is general enough and enables the use of any convenient form  $\mu$ . Since we are interested in a local volume preservation, we carefully design a form  $\mu$  defined over a volumetric domain  $D$  such that  $d\mu$  is a volumetric form for which  $\text{Volume}(D) = \int_D d\mu$ . Furthermore,  $\mu|_M$  reflects the local volume *underlying* the point  $p$  on surface  $M$ .

Let us construct a volumetric domain  $D$  over which  $\mu$  is defined (see Figure 11). The volume  $D$  approximates the original volume. We aim at preserving the volume of  $D$ , and in particular, its local volume. In the following, we define the meaning of local volume and its construction.

Denote by  $V$  the volume enclosed by surface  $M$ , that is,  $M = \partial V$ . Let  $\psi : M \times \mathbb{R} \rightarrow \mathbb{R}^3$  map a point  $p$  on the surface  $M$  to a parametric line emanating from  $p$ :  $\psi(p, t) = p - te_3(p)$ , where  $e_3$  is the normal pointing outward to the surface at  $p$ , and  $t$  is the parameter along this line.

Let  $\phi : M \rightarrow \mathbb{R}$  be a smooth function such that  $M' := \{\psi(p, \phi(p)), p \in M\} = \{p - \phi(p)e_3(p), p \in M\}$  is a smooth surface. Here,  $\phi$  represents the local depth of the volume element estimated at  $p$ .

Denote by  $V'$  the volume enclosed by  $M'$  (the green region in Figure 11), and let  $D = V \setminus V'$  be the volume enclosed between  $M$  and  $M'$ . Next, let  $(e_1, e_2, e_3)$  be an orthonormal frame such that its restriction to  $M = \partial V$  is a moving frame in the sense we defined in Section 3.

Denote by  $w_i$  the coframes of  $e_i$  in the volume  $D$ ,  $i = 1, 2, 3$ , that is, the linear functional satisfying  $w_i(e_j) = \delta_{i,j}$ , where  $\delta_{i,j}$  equals one if  $i = j$ , and otherwise equals zero. We construct  $\mu$  such that:

$$\begin{aligned} d\mu &= w_1 \wedge w_2 \wedge w_3 = dx_1 \wedge dx_2 \wedge dx_3, \\ \mu &= h \cdot w_1 \wedge w_2, \end{aligned} \quad (9)$$

where  $\wedge$  denotes the wedge product [Stoker 1989; do Carmo 1994; Ivey and Landsberg 2003].

The first requirement implies that  $\int_D d\mu = \text{Volume}(D)$ , and the second requirement means that  $\mu|_M$  depends only on the trajectory in the direction of the inward normal ( $-e_3$ ), as explained to follow. In order to calculate  $\mu$ , it is enough to find out  $h$  (given that the moving frames are known). Given these requirements, as shown in Appendix B,  $h$  satisfies the following first-order linear ODE,

$$\frac{\partial}{\partial e_3} h = 1 - h(\nabla \cdot e_3). \quad (10)$$

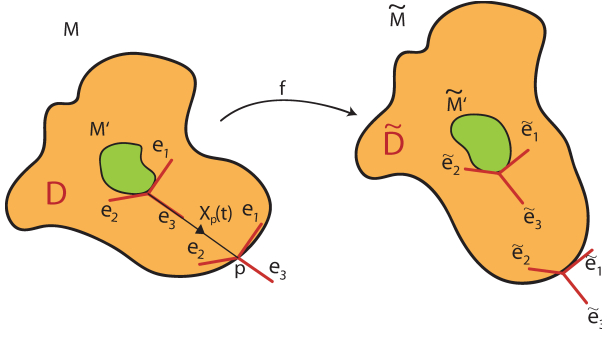


Fig. 11. The volume preservation setting.

Note that the operator  $\nabla \cdot e_3$  restricted to the surface is the mean curvature. The characteristic curves of this ODE are the trajectories in the direction of the normal vector field ( $e_3$ ) in  $D$ . Hence, the previous equation establishes an interesting connection between the mean curvature and the volume. This connection is the key observation to our volume correction method.

Thus, given a solution  $h$  to the ODE,  $\mu$  is of the form  $\mu = h \cdot w_1 \wedge w_2$ , and we have

$$\text{Volume}(D) = \int_{\partial D} h \, d\sigma = \int_{\partial V=M} h \, d\sigma - \int_{\partial V'=M'} h \, d\sigma, \quad (11)$$

where  $d\sigma = w_1 \wedge w_2$  is the area element. Since we can choose any initial values to  $h$ , we set it to zero on  $M'$ , and are left with

$$\text{Volume}(D) = \int_{\partial V=M} h \, d\sigma.$$

Let us now consider the two surfaces  $M$  and deformed isometric surface  $\tilde{M}$ . Similar to the preceding, we define a depth function  $\phi$ , and a corresponding surface  $\tilde{M}' = \{\tilde{p} - \phi(\tilde{p})\tilde{e}_3 | \tilde{p} \in \tilde{M}\}$ . Also we denote by  $\tilde{V}$  and  $\tilde{V}'$  the volume enclosed by  $\tilde{M}$  and  $\tilde{M}'$ , respectively, and  $\tilde{D} := \tilde{V} \setminus \tilde{V}'$  (see Figure 11).

Using Eq. (11) for  $\tilde{M}$  with  $h|_{\partial\tilde{V}'} = 0$ , we get:  $\text{Volume}(\tilde{D}) = \int_{\partial\tilde{V}} \tilde{h} \, d\tilde{\sigma}$ . Since the two surfaces  $M, \tilde{M}$  are isometric,  $d\tilde{\sigma} = d\sigma$ . By scaling the area element  $d\tilde{\sigma}$ , that is, scaling the moving frames on the surface by  $\kappa = (h/\tilde{h})^{1/2}$ , we get that the local volume of  $M$  is preserved in  $\tilde{M}$ . This assumes that  $\tilde{h}$  is not affected much by scale.

## 4.2 The Realization

As discussed earlier, the problem of volume correction is reduced to the problem of estimating  $h, \tilde{h}$  on the meshes  $M, \tilde{M}$ , respectively. Phrased differently, we should solve the ODE (Eq. (10)) with the initial condition  $h|_{\partial V'} = 0$  in  $D$ , and  $h|_{\partial\tilde{V}'} = 0$  in  $\tilde{D}$ . In the following, we describe the process for the mesh  $M$  (and similarly for  $\tilde{M}$ ).

Defining the volume  $D$  is equivalent to defining the function  $\phi$ . To each vertex  $p \in M$ , we attach a moving frame ( $e_1, e_2, e_3$ ), and we extend this into the volume  $D$  simply by translating the frame in the inward normal ( $-e_3$ ) direction. Ideally,  $\psi$  should be an injective map:  $\psi(\cdot, \phi(\cdot)) : M \rightarrow M'$ . In practice, we use the following considerations. We define the *local depth*, denoted by  $L(p)$  at a vertex  $p \in M$ , as the distance between  $p$  and the intersection of the line emanating from  $p$  in the inward normal ( $-e_3$ ) direction with the surface. In practice, we take the average of distances obtained by a narrow cone of straight lines from  $p$  (in a preprocess calculation). Denote by  $r_1 = 1/k_1, r_2 = 1/k_2$  the signed osculating

radii, where  $k_1$  and  $k_2$  are the corresponding discrete principle curvature at a point  $p$ . We choose  $\phi(p) = \min\{\alpha L(p), \beta(r_1)_+, \beta(r_2)_+\}$ , where  $(x)_+ = \infty$  for  $x \leq 0$  and  $(x)_+ = x$  for  $x > 0$ . Furthermore,  $\alpha \in (0, 1/2], \beta \in (0, 1)$  are constants which control the thickness of the volume  $D$  to be preserved. We mainly use  $\alpha = \beta = 1/2$  to approximate the whole volume. The reason for this definition of  $\phi$  lies in the fact that if one of the osculating radii is small and positive, then for (local) injectivity of  $\psi(p, \phi(p))$ , the local depth cannot exceed this value.

Note that the aforementioned are local computations which do not take into consideration global self-intersections. Also, to enable interactive time response, the values  $L(p)$  for the mesh  $\tilde{M}$  are taken to be as in  $M$ . This is equivalent to using the same local depth of the volumes  $D$  and  $\tilde{D}$ . During the interaction, the volume correction requires only local curvatures' estimation across the mesh.

Using the parametrizations of  $D$ ,  $\psi(p, t) \in D$ , where  $p \in M$  is fixed and  $t \in [0, \phi(p)]$ , we estimate the term  $\nabla \cdot e_3$  in the ODE (Eq. (10)) by

$$\nabla \cdot e_3(t) = \begin{cases} 0 & k_1=0=k_2 \\ \frac{1}{a_j+t} & k_j \neq 0, k_i=0, \{i,j\}=\{1,2\} \\ \frac{1}{a_1+t} + \frac{1}{a_2+t} & k_1 \neq 0, k_2 \neq 0 \end{cases}, \quad (12)$$

which corresponds to the position  $\psi(p, t)$  and  $a_i = r_i - \phi(p)$ ,  $i = 1, 2$ .

The rationale of this estimation is that it is enough to consider locally the surface by its osculating paraboloid and extending the local frame  $\{e_i\}_{i=1}^3$  in a natural way into the volume by translation along the inward normal direction. In this case,  $\nabla \cdot e_3$ , which is the trace of the differential of the normal map, is the mean curvature of the level surface  $\psi(p, t = \text{const})$ . Note that this value appears in our ODE for  $h$  (see Eq. (10)).

With the previous approximation, we can explicitly solve Eq. (10) on the characteristic curves. Characteristic curves are the trajectories in the direction of the normals,  $X_p(t) = p + (t - \phi(p))e_3(p)$ , starting from the surface  $M'$  and ending at the surface  $M$  (see Figure 11). Setting the the initial conditions  $h(0) = 0$  (0 on the surface  $M'$ ), we obtain the solution

$$h(t) = \begin{cases} t & k_1=0=k_2 \\ \frac{t^2/2+a_j t}{a_j+t} & k_j \neq 0, k_i=0, \{i,j\}=\{1,2\} \\ \frac{t^3/3+(a_1+a_2)t^2/2+a_1 a_2 t}{(a_1+t)(a_2+t)} & k_1 \neq 0, k_2 \neq 0 \end{cases}. \quad (13)$$

For each vertex  $p \in M$  and its corresponding vertex  $\tilde{p} \in \tilde{M}$ , we approximate the scalar fields  $h$  and  $\tilde{h}$  on the two surfaces by evaluating Eq. (13) at  $t = \phi(p)$  and  $t = \phi(\tilde{p})$ , that is,  $h(p) = h(\phi(p))$  and  $\tilde{h}(\tilde{p}) = h(\phi(\tilde{p}))$ . Finally, we compute the scaling factor for vertex  $\tilde{p} \in \tilde{M}$  as  $(h(p)/\tilde{h}(\tilde{p}))^{1/2}$ , and use this to scale the rotated frames. Then we use these moving frames to reconstruct the mesh [Lipman et al. 2005], as elaborated in Section 5.

## 5. IMPLEMENTATION AND RESULTS

We have integrated our shape- and volume-preserving technique into an interactive system. The system accepts a mesh  $M$  and a set of constraints  $C \subset M$  which defines the geometric deformation. There are two types of constraints  $S \cup H = C$ : The set  $S$  is the *static* set of vertices, with rotations set to identity, and  $H$  is the *handle* set, over which the user defines the rotations. In Figures 6, 8, and 10, the handle set is colored yellow and the static set is colored green.



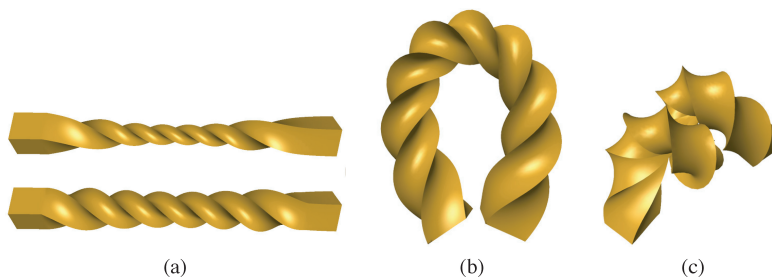


Fig. 12. The volume correction algorithm is applied to a twisted bar. A rotation of approximately  $4\pi$  in one step is obtained by applying our technique, without volume correction in (a) top, and with volume correction in (a) bottom. Applying a rotation of  $4\pi$  and then another rotation of  $3\pi/4$  around another rotation axis yields (b). Moreover, (c) shows the result of applying one big rotation of  $3\pi$ , together with position constraints, to form a helical shape.

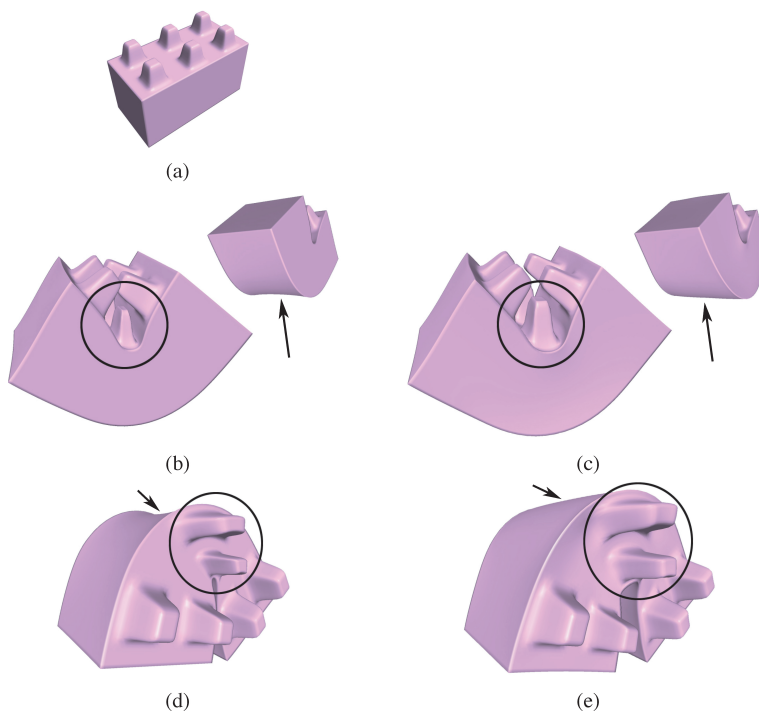


Fig. 13. The volume correction algorithm is applied to a Lego piece model (a). In (b),(d) without volume correction and in (c),(e) with volume correction.

In the preprocess stage, we: (i) create and factorize the Laplace-Beltrami matrix of the region of interest of the mesh, and (ii) calculate the local depth field  $L$  of the mesh.

During interaction:

—*the rotation field  $R : M \rightarrow SO(3)$  is calculated:*

—In the case of *bending* with a single rotation axis, the Laplace-Beltrami factorization is used to solve for the rotation angle  $\theta^1$  (see Eq. (6)).

—Otherwise, the Laplace-Beltrami factorization is used to solve for conformal parameters  $(\eta^1, \eta^2, \eta^3)$  (see Eqs. (6) and (8)). For example, see Figure 4, where at each vertex in the handle (yellow), the rotation is around the tangent to the curve. Optional: Further iterate using Eq. (8).

—*The rotations are applied to the moving frames at each vertex, and the new mesh  $M$  is reconstructed by the difference equations*

[Lipman et al. 2005]:

$$\tilde{p}_j - \tilde{p}_i = A_{i,j}\tilde{e}_1^i + B_{i,j}\tilde{e}_2^i + C_{i,j}\tilde{e}_3^i, \quad (14)$$

where  $(i, j)$  is an edge of the mesh,  $\tilde{p}_i$  are the new unknown position of vertex  $i$ , and  $(\tilde{e}_1^i, \tilde{e}_2^i, \tilde{e}_3^i)$  denotes the rotated moving frame at vertex  $i$ . Moreover,  $A_{i,j}, B_{i,j}, C_{i,j}$  are the coefficients of  $p_j - p_i$  in the moving frame  $(e_1^i, e_2^i, e_3^i)$  at  $p_i$  in  $M$ . As in Lipman et al. [2005], the solution of the system (14) is done in the least-squares sense.

—*The scaling factor for volume correction is calculated:*

—Calculate the  $h$ -fields by Eq. (13):  $h$  and  $\tilde{h}$ , of  $M$  and  $\tilde{M}$ , respectively. The evaluation of Eq. (13) uses the precomputed local depth  $L$ , and the local discrete curvature are computed over the deformed mesh.

—The scale factor is set to be  $(h/\tilde{h})^{1/2}$ .

—*The (rotated) moving frames of  $M$  are scaled by the scaling factor and the mesh is reconstructed.*

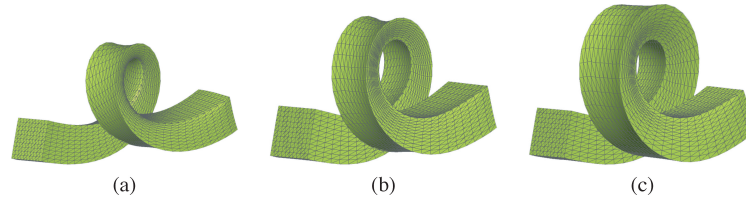


Fig. 14. Rotation of over  $2\pi$  is applied to a bar. In (a), the technique of Lipman et al. [2005] is applied three times with  $2\pi/3$  in each step. In (b), the shape-preserving isometric deformation is applied in one single step; (c) a volume correction is applied to (b).

There are some important implementation issues. First, for irregular meshes, it is useful to use other discrete Laplacian operators. We have also integrated the discrete Laplacian operator as presented in Taubin [1995] into our system and got better results on highly-irregular meshes (e.g., see Figure 17). Second, we note that the deformation which is defined by the field of rotations on moving frames is invariant to the actual choice of moving frames. Hence, any choice of local frames as moving frames will do. Third, positional constraints are forced, as in Lipman et al. [2005], by adding them to the positional reconstruction system (14).

The isometric shape-preserving technique requires solving sparse linear systems. Similarly to the technique of Lipman et al. [2005], we use a sparse Cholesky decomposition [Toledo 2003] once per definition of a region of interest (ROI). During interaction, only back-substitution is needed. The volume correction is slower where the bottleneck is the computation of the discrete curvature, which is directly related to the number of vertices of the surface mesh. For example, meshes of sizes 2.2K, 8.5K, and 86.5K vertices require 0.14, 1.03, and 11.66 seconds for factorization, 0.016, 0.047, and 0.66 seconds for back-substitution, and 0.05, 0.17, and 1.9 seconds for volume correction, respectively, on an Intel P4/3.0 GHz.

To demonstrate the performance of our technique, we show extremely large deformations in Figures 5, 15, and 17. To visualize the quality of the deformation, we color coded the difference between the mean curvature across the surface before and after the deformation. Figure 8 demonstrates the shape preservation under a large deformation. In Figure 9, we compare our method to that of Sorkine et al. [2004]. Note that Sorkine’s method doesn’t distribute the rotations uniformly. However, it should be noted that their method incorporates positional constraints.

Figure 14 shows a bar rotated by over  $2\pi$  radians. In (a), the bar is rotated by integrating three steps (of approximately  $2\pi/3$  degree, each), using the technique of Lipman et al. [2005]. The result in (b) is achieved by a single step using our technique. In (c), a volume correction is applied to the bent bar. In Figure 12, a bar is twisted by an extreme rotation of approximately  $4\pi$  at one step (a); in (b) the volume correction is applied; and in (c) and (d) one more deformation is applied. Figure 16 shows a volume loss (a), and correction (b), of a twisted Armadillo model. Since local volume-preservation implies global volume-preservation, we also achieve global volume-preservation, to some extent. Particularly in Table I, we have measured the relative change of volume, that is,  $|volume_{new} - volume_{old}|/volume_{old}$ , of two meshes under various deformations. As can be seen, for medium-scale deformations, the volume correction algorithm reduced the volume change by an order of magnitude. Another example of the volume correction algorithm is presented in Figure 13, where it can be seen that the method is correcting the detail’s volume as well as the global volume.

Interesting editing operators can be obtained by nontrivial static and handle sets. Figure 7 illustrates the effect of the rectangular

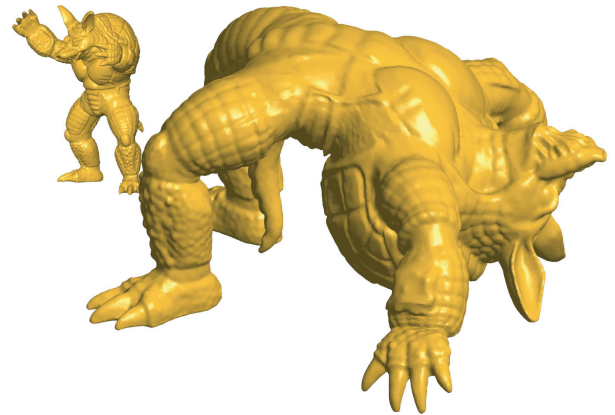


Fig. 15. The body of the Armadillo model is bent by  $\pi$  radians and the hands are further bent to create a bridge-like pose. Note the preservation of details and volume under the deformation.

curve handle with different boundary conditions over a simple plane, resulting in shape-preserving (planar) isometric deformations. Figure 6 shows a smooth wavy shape created by bending a plane, and Figure 4 shows a bumpy ball with a pinched-like deformation.

## 6. CONCLUSIONS

We have presented a method for shape-preserving deformation. The approach we have taken in this article reformulates the preservation of shape by means of a complete representation of local rigid-invariant descriptors. In essence, our method aims at the preservation of the two fundamental forms. Isometries preserve the first fundamental form, that is, the area and angle, and among the isometries, we look further for the one that minimizes changes of the second fundamental form. The minimization is practically linear, thanks to the reduction of the problem to a Dirichlet-type functional on a rotation field over the mesh.

Since isometric deformations can cause volume changes of closed surfaces, we have established a relation between the local volume and the surface curvature, from which we derived a local scaling field that can be applied to surface elements to correct local volume changes. An interesting consequence is that changes in the curvature data of the surface can provide a good means to control volume changes.

Note that we cannot preserve simultaneously the surface area and volume of an object. An exciting avenue for future research is to investigate other complete local surface descriptors, whose preservation yields a shape preservation of both surface and volume.

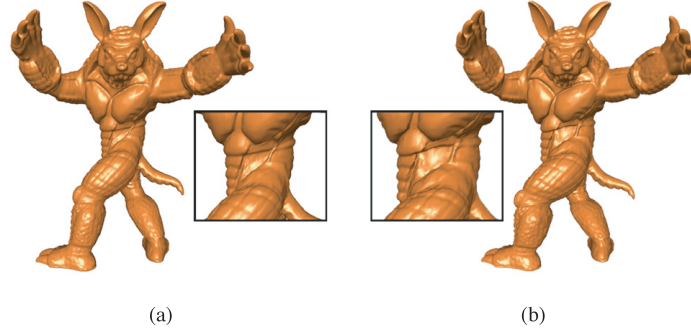


Fig. 16. The Armadillo model is twisted by  $8\pi/9$  radians. Shape-preserving deformations, without volume correction (a) and with volume correction (b).

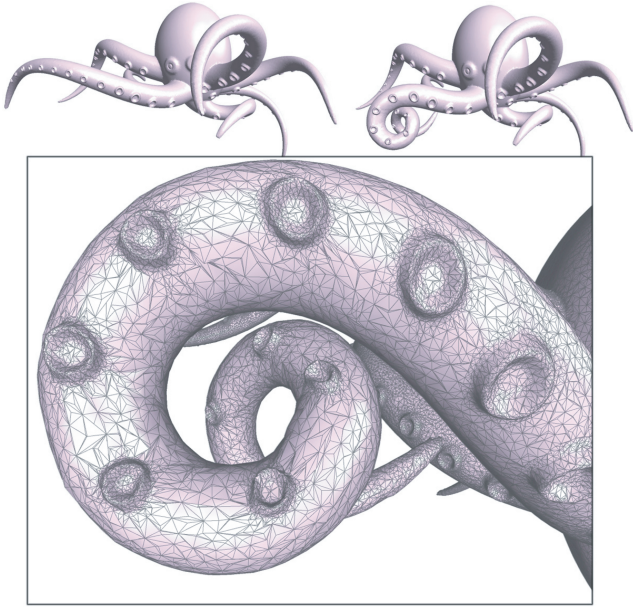


Fig. 17. The tip of the tentacle of the octopus is rotated by  $3\pi$  radians. Note the preservation of details, despite highly-irregular triangulation of the mesh.

## APPENDIXES

### APPENDIX A

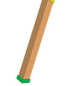


In this appendix we prove the relation  $\|H - \tilde{H}\|_F^2 = 1/2\|\nabla R\|_F^2$ . In order to do so, we will use standard exterior calculus of differential forms [Stoker 1989; do Carmo 1994; Ivey and Landsberg 2003]. We build upon the notation introduced in Section 3. The general setting is illustrated in Figure 3.

Let  $g : U \subset \mathbb{R}^2 \rightarrow V \subset M$  be a coordinate map. Note that  $f \circ g : U \subset \mathbb{R}^2 \rightarrow f(V) \subset \mathbb{R}^3$  is a coordinate map of  $\tilde{M}$ . Next, define the differential one-forms on  $U \subset \mathbb{R}^2$ ,  $w_i, w_{i,j}, i, j = 1, 2, 3$  by the two relations

$$dg(\cdot) = \sum_{i=1}^3 w_i(\cdot)e_i, \quad de_i(\cdot) = \sum_{j=1}^3 w_{i,j}(\cdot)e_j. \quad (15)$$

Note that these relations describe the change of frame and its position, coded in the frame itself. Also note that  $w_{i,j} = -w_{j,i}$ , as

Table I. The Relative Change in Volume

| Model  | Rotation | No Volume Correction | With Volume Correction |
|--|----------|----------------------|------------------------|
|   | $\pi/2$  | 0.0473               | 0.00267                |
|  | $\pi$    | 0.143                | 0.00333                |
|  | $2\pi$   | 0.37                 | 0.00173                |
|  | $3\pi$   | 0.53                 | 0.0533                 |
|   | $\pi/4$  | 0.0164               | 0.00663                |
|  | $\pi/2$  | 0.0412               | 0.00971                |
|  | $\pi$    | 0.143                | 0.0316                 |
|  | $3\pi/2$ | 0.260                | 0.0704                 |
|  | $\pi/6$  | 0.023                | 0.0025                 |
|  | $\pi/3$  | 0.083                | 0.0057                 |
|  | $2\pi/3$ | 0.267                | 0.1                    |
|  | $\pi$    | 0.435                | 0.24                   |

These volume changes result from the shape-preserving isometric deformation, with and without volume correction: The *Armadillo* and *bar* models, which consist of 170K and 4K polygons, respectively, are deformed by bending operators with several prescribed angles. The handle and static sets are in yellow and green, respectively.

can be proved by differentiating  $\langle e_i, e_j \rangle = \delta_{i,j}$  and using Eq. (15). Define the differential one-forms  $\tilde{w}_i, \tilde{w}_{i,j}, i = 1, 2, 3$  by

$$d(f \circ g)(\cdot) = \sum_{i=1}^3 \tilde{w}_i(\cdot)\tilde{e}_i \quad d\tilde{e}_i(\cdot) = \sum_{j=1}^3 \tilde{w}_{i,j}(\cdot)\tilde{e}_j.$$

It follows from the preceding that  $w_i = \tilde{w}_i$ . To prove this, note that  $\sum_{i=1}^3 \tilde{w}_i(dg^{-1}(e_j))\tilde{e}_i = d(f \circ g)(dg^{-1}(e_j)) = df(e_j) = \tilde{e}_j$ , and use the linear independence of  $\tilde{e}_j$  to get  $\tilde{w}_i(dg^{-1}(e_j)) = \delta_{i,j} = w_i(dg^{-1}(e_j))$ .

Since we have chosen the moving frame such that  $e_3$  is normal to the surface, the one-form  $w_3 = 0$ . To see this, note that due to the first equation in Eq. (15),  $T_p M \ni dg(\xi) = \sum_{i=1}^3 w_i(\xi)e_i, \xi \in T_{g^{-1}(p)}\mathbb{R}^2 = \mathbb{R}^2$ , so necessarily  $w_3(\xi) = 0$  for all  $\xi$ . From the structure equations in Lemma C.2, we then have  $0 = w_1 \wedge w_{1,3} + w_2 \wedge w_{2,3}$ , and using the Lemma of Cartan C.3, we get

$$w_{1,3} = h_{1,1}w_1 + h_{1,2}w_2, \quad w_{2,3} = h_{2,1}w_1 + h_{2,2}w_2. \quad (16)$$

Here,  $h_{i,j}, i, j = 1, 2$  are the coefficients of the differential of the normal map, that is,  $de_3 : T_p M \rightarrow T_p M$ , in the basis  $e_1, e_2$  (as introduced in Section 3). The second fundamental form can then be written by  $\sum_{i,j} h_{i,j}w_i w_j, i, j = 1, 2$ . Also note that  $h_{1,2} = h_{2,1}$ . From the fact that  $\tilde{w}_i = w_i$ , we also have  $0 = w_1 \wedge \tilde{w}_{1,3} + w_2 \wedge \tilde{w}_{2,3}$ , and using the Cartan Lemma C.3 again, we get

$$\tilde{w}_{1,3} = \tilde{h}_{1,1}w_1 + \tilde{h}_{1,2}w_2, \quad \tilde{w}_{2,3} = \tilde{h}_{2,1}w_1 + \tilde{h}_{2,2}w_2, \quad (17)$$

where now  $\tilde{h}_{i,j}$ ,  $i, j = 1, 2$  are the coefficients of  $d\tilde{e}_3$  in  $\tilde{e}_j$ ,  $j = 1, 2$ . Next, we use the local distance function  $dist_{M,f}$ , as defined in Eq. (1).

As mentioned before, we consider a rotation field  $R : M \rightarrow SO(3)$ , where  $SO(3)$  is the rotation matrix group on  $\mathbb{R}^3$  embedded in  $\mathbb{R}^9$  with the induced metric. Moreover,  $R \in SO(3)$  is defined by the relations  $Re_i = \tilde{e}_i$ ,  $i = 1, 2, 3$ . Using these relations we have

$$R \sum_j \tilde{w}_{i,j} e_j = d\tilde{e}_j = dRe_i + Rde_i = dRe_i + R \sum_j w_{i,j} e_j.$$

Rearranging the previous leftmost and rightmost terms, we get

$$R^{-1}dRe_i = \sum_j \Delta w_{i,j} e_j, \quad (18)$$

where  $\Delta w_{i,j} = \tilde{w}_{i,j} - w_{i,j}$ . In matrix notation we can rewrite Eq. (18) as

$$dR = RESE^t, \quad (19)$$

where  $E = (e_1, e_2, e_3)$  ( $e_i$  is a column vector), and  $S = (\Delta w_{i,j})_{j,i}$ . Since  $w_{i,i} = 0$  and  $w_{1,2} = \tilde{w}_{1,2}$ , we have

$$S = \begin{pmatrix} 0 & 0 & -\Delta w_{1,3} \\ 0 & 0 & -\Delta w_{2,3} \\ \Delta w_{1,3} & \Delta w_{2,3} & 0 \end{pmatrix}.$$

The fact that  $w_{1,2} = \tilde{w}_{1,2}$  can be understood from the Lemma of Levi-Civita C.4 and the structure equations in Lemma C.2. From Eqs. (16) and (17) we have

$$\begin{aligned} \Delta w_{1,3} &= \Delta h_{1,1}w_1 + \Delta h_{1,2}w_2, \\ \Delta w_{2,3} &= \Delta h_{2,1}w_1 + \Delta h_{2,2}w_2. \end{aligned} \quad (20)$$

Therefore

$$S(e_1) = \begin{pmatrix} 0 & 0 & -\Delta h_{1,1} \\ 0 & 0 & -\Delta h_{2,1} \\ \Delta h_{1,1} & \Delta h_{2,1} & 0 \end{pmatrix}, \quad S(e_2) = \begin{pmatrix} 0 & 0 & -\Delta h_{1,2} \\ 0 & 0 & -\Delta h_{2,2} \\ \Delta h_{1,2} & \Delta h_{2,2} & 0 \end{pmatrix}.$$

Note that the induced  $\mathbb{R}^9$  norm on the rotation matrix group is the Frobenius norm. Next, let us calculate  $\|\nabla R\|_F^2 = \|dR\|_F^2 = \sum_{i,j=1}^3 \langle dR_{i,j}, dR_{i,j} \rangle$ , where  $R = (R_{i,j})$  are the entries in the rotation matrix  $R$ . Writing  $dR_{i,j}$  in the basis  $w_1, w_2$ , we have  $dR_{i,j} = R_{i,j}^1 w_1 + R_{i,j}^2 w_2$  so  $\langle dR_{i,j}, dR_{i,j} \rangle = (R_{i,j}^1)^2 + (R_{i,j}^2)^2$ . Putting it all together, we have  $\|dR\|_F^2 = \sum_{i,j} (R_{i,j}^1)^2 + (R_{i,j}^2)^2 = \|dR(e_1)\|_F^2 + \|dR(e_2)\|_F^2$ . Next,  $\|dR(e_i)\|_F^2 = \text{trace}(RES(e_i)E^tES(e_i)^t(RE)^t) = \|S(e_i)\|_F^2$  by the invariance of the trace operator under similarity transformation. Finally,

$$\sum_{i,j=1}^2 (\Delta h_{i,j})^2 = \frac{1}{2} \|\nabla R\|_F^2.$$

## APPENDIX B

Using the notation of Section 4, we now derive the two-form  $\mu$  in the volume  $D$  such that the requirement (9) is satisfied. Let  $(b_1, b_2, b_3)$  denote the standard basis in  $\mathbb{R}^3$ , and denote by  $M = (m_{ij})_{i,j=1}^3 \in \mathbb{R}^{3,3}$  the matrix such that

$$(e_1, e_2, e_3) = (b_1, b_2, b_3)M \quad (21)$$

$$(w_1, w_2, w_3) = (dx_1, dx_2, dx_3)M, \quad (22)$$

where  $dx_i$  is the coframe of the (constant) frame  $b_i$ ,  $i = 1, 2, 3$ . Next, we span  $\mu$  in the basis of two-forms:  $\mu = \chi dx_1 \wedge dx_2 +$

$\lambda dx_1 \wedge dx_3 + \xi dx_2 \wedge dx_3$ . From the first requirement on  $\mu$ :

$$dx_1 \wedge dx_2 \wedge dx_3 = d\mu = (\chi_{x_3} - \lambda_{x_2} + \xi_{x_1})dx_1 \wedge dx_2 \wedge dx_3,$$

implying

$$1 = (\chi_{x_3} - \lambda_{x_2} + \xi_{x_1}), \quad (23)$$

where the subscripts  $x_i$  denote differentiation with respect to  $x_i$ .

For the second requirement,  $\mu = h \cdot w_1 \wedge w_2$ ,

$$\chi dx_1 \wedge dx_2 + \lambda dx_1 \wedge dx_3 + \xi dx_2 \wedge dx_3 = \mu =$$

$$h(m_{11}dx_1 + m_{21}dx_2 + m_{31}dx_3) \wedge (m_{12}dx_1 + m_{22}dx_2 + m_{32}dx_3),$$

and if we denote  $M_{ij} = \det \begin{pmatrix} m_{i1} & m_{i2} \\ m_{j1} & m_{j2} \end{pmatrix}$ , then the righthand side of the last equation becomes

$$h\{M_{12}dx_1 \wedge dx_2 + M_{13}dx_1 \wedge dx_3 + M_{23}dx_2 \wedge dx_3\},$$

and therefore, by equating coefficients of the representation,

$$\chi = hM_{12} \quad \lambda = hM_{13} \quad \xi = hM_{23}. \quad (24)$$

Using (24) in (23) and noting that in the basis  $b_i$ ,  $e_3 = e_1 \times e_2 = (M_{23}, -M_{13}, M_{12})$ , we get

$$\nabla h \cdot e_3 = 1 - h(\nabla \cdot e_3),$$

which is the desired result.

## APPENDIX C

LEMMA C.1. *Definition (1) is independent of the choice of moving frame.*

PROOF. We use the notation presented in Section 3. Denote by  $E = (e_1, e_2, e_3)$  and  $E^o = (e_1^o, e_2^o, e_3)$  two local choices of moving frames, and denote by  $H$  ( $\tilde{H}$ ) the matrix which represents the shape operator  $de_3$  ( $d\tilde{e}_3$ ) in the basis  $e_1, e_2$  of  $T_pM$  ( $\tilde{e}_1, \tilde{e}_2$  of  $T_{f(p)}\tilde{M}$ ).

Then,  $H^o = M^t H M$  is the matrix of  $de_3$  in the basis  $E^o$ , where  $E^o = E M$ . We defined  $\tilde{E} = (df)E$ , therefore,  $\tilde{E}^o = (df)E^o = (df)EM = \tilde{E}M$ , that is, the basis  $E^o$ , that is, the basis  $E^o$ , defines by the isomorphism  $df$  a new basis of  $T_{f(p)}\tilde{M}$  which (as  $E$  and  $E^o$ ) satisfies  $\tilde{E}^o = \tilde{E}M$ , so the matrix representing  $\tilde{H}$  in the basis  $\tilde{E}^o$  is  $M^t \tilde{H} M$ . Therefore,

$$dist_{M,f}^{E^o}(p) = \|H - \tilde{H}\|_F^2 = \|M^t(H - \tilde{H})M\|_F^2 = dist_{M,f}^{E^o}(p),$$

so the function  $dist_{M,f}$  is invariant to the choice of the moving frames and is only dependent on the surface  $M$  and isometry  $f$ .  $\square$

LEMMA C.2 (THE STRUCTURE EQUATIONS). *Let  $V \subset M$  be an open set of  $M$ , and assume  $(e_1, e_2, e_3)$  to be a smooth orthonormal moving frame defined on  $M$ . Then the one-forms defined by Eq. (15) satisfy*

$$dw_i = \sum_k w_k \wedge w_{k,i},$$

$$dw_{i,j} = \sum_k w_{i,k} \wedge w_{k,j}, \quad i, j, k = 1, 2, 3.$$

LEMMA C.3 (CARTAN'S LEMMA). *Let  $V^n$  be a vector space of dimension  $n$ , and let  $w_1, \dots, w_r : V^n \rightarrow \mathbb{R}$ ,  $r \leq n$ , be one-forms in  $V$  that are linearly independent. Assume there exist forms  $\theta_1, \dots, \theta_r : V \rightarrow \mathbb{R}$  such that  $\sum_{i=1}^r w_i \wedge \theta_i = 0$ . Then*

$$\theta_i = \sum_j a_{i,j} w_j, \quad a_{i,j} = a_{j,i}.$$

LEMMA C.4 (LEMMA OF LEVI-CIVITA). *Let  $M$  be a Riemannian two-dimensional manifold. Let  $V \subset M$  be an open set where a moving orthonormal frame  $\{e_1, e_2\}$  is defined, and let  $\{w_1, w_2\}$  be the associated coframe. Then, there exists a unique one-form  $w_{1,2} = -w_{2,1}$  such that*

$$dw_1 = w_{1,2} \wedge w_2 \quad dw_2 = w_{2,1} \wedge w_1.$$

## APPENDIX D

In this appendix we describe the two parametrizations we use for the Euclidian rotation group  $SO(3)$ . First, the *orthogonal parametrization*

$$\theta^{orth} : (\theta^1, \theta^2, \theta^3) \subset [0, 2\pi) \times [0, \pi) \times [0, 2\pi) \mapsto SO(3) \subset \mathbb{R}^9 \quad (25)$$

is defined as the composition of the two maps:

$$(\theta^1, \theta^2, \theta^3) \mapsto \begin{pmatrix} \sin(\theta^1/2)\sin(\theta^2)\sin(\theta^3) \\ \sin(\theta^1/2)\sin(\theta^2)\cos(\theta^3) \\ \sin(\theta^1/2)\cos(\theta^2) \\ \cos(\theta^1/2) \end{pmatrix},$$

and

$$\begin{pmatrix} x \\ y \\ z \\ w \end{pmatrix} \mapsto \begin{pmatrix} 1-2y^2-2z^2 & 2xy+2wz & 2xz-2wy \\ 2xy-2wz & 1-2x^2-2z^2 & 2yz+2wx \\ 2xz+2wy & 2yz-2wx & 1-2x^2-2y^2 \end{pmatrix}, \quad (26)$$

where  $(x \ y \ z \ w)^T$  is a quaternion. Using this parametrization, we get the induced metric

$$G = 2\text{Diag}(1 \ 4 \sin^2(\theta^1/2) \ 4 \sin^2(\theta^1/2) \sin^2(\theta^2)),$$

where  $\text{Diag}(d_0, \dots, d_n)$  denotes the diagonal matrix with diagonal entries  $d_0, \dots, d_n$ .

Second, we describe the *conformal parametrization*

$$\eta^{conf} : (\eta^1, \eta^2, \eta^3) \subset \mathbb{R}^3 \mapsto SO(3) \subset \mathbb{R}^9, \quad (27)$$

defined by composition of the map  $(\eta^1, \eta^2, \eta^3) \mapsto (\frac{4\eta^1}{\|\bar{\eta}\|^2+4}, \frac{4\eta^2}{\|\bar{\eta}\|^2+4}, \frac{4\eta^3}{\|\bar{\eta}\|^2+4}, \frac{4-\|\bar{\eta}\|^2}{\|\bar{\eta}\|^2+4})$  with map (26). The first map is known as the stereographic map. This parametrization gives us the induced metric  $G = 128w(\bar{\eta})I$ , where  $w(\bar{\eta}) = 1/(\|\bar{\eta}\|^2 + 4)^2$  and  $I$  denotes the  $3 \times 3$  identity matrix.

## APPENDIX E

In this section we'll show that under the conformal parameter (27), Eq. (3) boils down to Eq. (5).

As detailed in Appendix D, the induced metric in the conformal coordinate system is  $G = w(\bar{\eta})I$ , where  $w(\bar{\eta}) = 128/(\|\bar{\eta}\|^2 + 4)^2$  and  $I$  denotes the  $3 \times 3$  identity matrix. Denote by  $R_\eta = (\eta_1, \eta_2, \eta_3) := \eta_{conf}^{-1}R : M \mapsto \mathbb{R}^3$ , then

$$\|dR\|_F^2 = \|d(R_\eta)\|_G^2.$$

Next, since  $(e_1, e_2)$  is an orthonormal basis of the tangent plane  $T_p M$ ,

$$\|d(R_\eta)\|_G^2 = \text{trace}(\nabla R_\eta)^T G (\nabla R_\eta) = w(\bar{\eta})(|\nabla \eta^1|^2 + |\nabla \eta^2|^2 + |\nabla \eta^3|^2) = w(\bar{\eta})\|\nabla \bar{\eta}\|^2.$$

Next, let us show that using the piecewise-linear finite element approach to discretize Eq. (5), we obtain Eq. (7). In the notation of

Section 3.3, we integrate Eq. (5) on each triangle  $T_j$  as a linear transformation, for example,

$$\int_{T_i} \frac{1}{w(\bar{\eta})} \|\nabla \eta^l\|^2 d\sigma = \frac{1}{2\text{area}(T_i)} \sum_{j=1}^3 \cot \gamma_{ij} |\eta_{ij}^l - \eta_{i_j}^l|^2 \int_{T_i} \frac{1}{w(\bar{\eta})} d\sigma.$$

Using linear approximation to the integrand, we get:

$$\int_{T_i} \frac{1}{w(\bar{\eta})} d\sigma = \frac{\text{area}(T_i)}{3} (w(\bar{\eta}_{i_1}) + w(\bar{\eta}_{i_2}) + w(\bar{\eta}_{i_3})).$$

Combining the aforementioned, we get Eq. (7).

## REFERENCES

- ALEXA, M., COHEN-OR, D., AND LEVIN, D. 2000. As Rigid-As-Possible shape interpolation. In *Proceedings of the ACM SIGGRAPH Conference*. 157–164.
- ANGELIDIS, A., CANI, M.-P., WYVILL, G., AND KING, S. 2004. Swirling-Sweepers: Constant volume modeling. In *Proceedings of the Pacific Graphics Conference*. Korea.
- AUBERT, F. AND BECHMANN, D. 1997. Volume-Preserving space deformation. *Comput. Graph.* 21, 5, 625–639.
- BATHE, K. J. 1982. *Finite Element Procedures in Engineering Analysis*. Prentice-Hall, Upper Saddle River, NJ.
- BOTSCH, M. AND KOBBELT, L. 2003. Multiresolution surface representation based on displacement volumes. *Comput. Graph. Forum (Eurographics)* 22, 3, 483–491.
- BOTSCH, M. AND KOBBELT, L. 2004. An intuitive framework for real-time freeform modeling. *ACM Trans. Graph.* 23, 3, 630–634.
- BOTSCH, M., PAULY, M., GROSS, M., AND KOBBELT, L. 2006. Primo: Coupled prisms for intuitive surface modeling. In *Eurographics Symposium in Geometry Processing*. 11–20.
- COHEN-OR, D., LEVIN, D., AND SOLOMOVICI, A. 1998. Three-Dimensional distance field metamorphosis. *ACM Trans. Graph.* 17, 2, 116–141.
- DO CARMO, M. P. 1994. *Differential Forms and Applications*. Springer Verlag.
- FLOATER, M. S. 2003. Mean value coordinates. *Comput. Aided Geom. Des.* 20, 1, 19–27.
- HIROTA, G., MAHESHWARI, R., AND LIN, M. C. 1999. Fast volume preserving free form deformation using multi-level optimization. In *Proceedings of the Solid Modeling and Applications Conference*. 234–245.
- HUANG, J., SHI, X., LIU, X., ZHOU, K., WEI, L.-Y., TENG, S.-H., BAO, H., GUO, B., AND SHUM, H.-Y. 2006. Subspace gradient domain mesh deformation. *ACM Trans. Graph.* 25, 3, 1126–1134.
- IGARASHI, T., MOSCOVICH, T., AND HUGHES, J. F. 2005. As-Rigid-As-Possible shape manipulation. *ACM Trans. Graph.* 24, 3, 1134–1141.
- IVEY, T. A. AND LANDSBERG, J. M. 2003. *Cartan for Beginners: Differential Geometry Via Moving Frames and Exterior Differential Systems*. American Mathematical Society, Boston.
- JU, T., SCHAEFER, S., AND WARREN, J. 2005. Mean value coordinates for closed triangular meshes. *ACM Trans. Graph.* 24, 3, 561–566.
- KOBBELT, L., CAMPAGNA, S., VORSATZ, J., AND SEIDEL, H.-P. 1998. Interactive multi-resolution modeling on arbitrary meshes. In *SIGGRAPH: Proceedings of the 25th Annual Conference on Computer Graphics and Interactive Techniques*. 105–114.
- LIPMAN, Y., SORKINE, O., COHEN-OR, D., LEVIN, D., RÖSSL, C., AND SEIDEL, H.-P. 2004. Differential coordinates for interactive mesh editing. In *Proceedings of the Shape Modeling International Conference*. 181–190.

- LIPMAN, Y., SORKINE, O., LEVIN, D., AND COHEN-OR, D. 2005. Linear rotation-invariant coordinates for meshes. In *Proceedings of the ACM SIGGRAPH Conference*. 479–487.
- MULLER, M., DORSEY, J., MCMILLAN, L., JAGNOW, R., AND CUTLER, B. 2002. Stable real-time deformations. In *SCA: Proceedings of the 2002 ACM SIGGRAPH/Eurographics Symposium on Computer Animation*. 49–54.
- PINKALL, U. AND POLTHIER, K. 1993. Computing discrete minimal surfaces and their conjugates. *Exper. Math.* 2, 15–36.
- POLTHIER, K. 2005. Computational aspects of discrete minimal surfaces. In *Global Theory of Minimal Surfaces, Proceedings of the Clay Mathematics Institute Summer School*.
- RAPPAPORT, A., SHEFFER, A., AND BERCOVIER, M. 1995. Volume preserving free-form solid. In *Proceedings of the Solid Modeling and Applications Conference*. 361–372.
- SEDEBERG, T. W., GAO, P., WANG, G., AND MU, H. 1993. 2-D shape blending: An intrinsic solution to the vertex path problem. In *Proceedings of the SIGGRAPH Conference*. 15–18.
- SORKINE, O., LIPMAN, Y., COHEN-OR, D., ALEXA, M., RÖSSL, C., AND SEIDEL, H.-P. 2004. Laplacian surface editing. In *Proceedings of the Eurographics/ACM SIGGRAPH Symposium on Geometry Processing*. Eurographics Association, 179–188.
- STOKER, J. J. 1989. *Differential Geometry*. Wiley, New York.
- TAUBIN, G. 1995. A signal processing approach to fair surface design. In *Proceedings of the ACM SIGGRAPH Conference*. 351–358.
- VON FUNCK, W., THEISEL, H., AND SEIDEL, H.-P. 2006. Vector field based shape deformations. *ACM Trans. Graph.* 25, 3, 1118–1125.
- XU, D., ZHANG, H., WANG, Q., AND BAO, H. 2005. Poisson shape interpolation. In *SPM: Proceedings of the ACM Symposium on Solid and Physical Modeling*. 267–274.
- YU, Y., ZHOU, K., XU, D., SHI, X., BAO, H., GUO, B., AND SHUM, H.-Y. 2004. Mesh editing with poisson-based gradient field manipulation. *ACM Trans. Graph.* 23, 3, 644–651.
- ZAYER, R., RÖSSL, C., KARNI, Z., AND SEIDEL, H.-P. 2005. Harmonic guidance for surface deformation. In *Computer Graphics Forum, Proceedings of Eurographics Conference*, vol. 24. Eurographics, Blackwell, Dublin.
- ZHOU, K., HUANG, J., SNYDER, J., LIU, X., BAO, H., GUO, B., AND SHUM, H.-Y. 2005. Large mesh deformation using the volumetric graph laplacian. *ACM Trans. Graph.* 24, 3, 496–503.

Received June 2006; accepted October 2006